Layered monophosphate tungsten bronzes [Ba(PO4)2]WmO3m-3: 2D-metals with locked charge-density-wave instabilities

Hicham Nimoh, Angel Arevalo Lopez, Marielle Huvé, Claire Minaud, Andrés Cano, Robert Glaum, Olivier Mentre

How to cite: *Angew. Chem. Int. Ed.* **2023,** *62,* e202302049
doi.org/10.1002/anie.202302049

Solid-State Chemistry | Hot Paper

Layered Monophosphate Tungsten Bronzes $[Ba(PO_4)_2]W_mO_{3m-3}$: 2D Metals with Locked Charge-Density-Wave Instabilities

Hicham Nimoh, Angel Moisés Arévalo-López, Marielle Huvé, Claire Minaud, Andrés Cano, Robert Glaum, and Olivier Mentré**

Abstract: Phosphate tungsten and molybenum bronzes represent an outstanding class of materials displaying textbook examples of charge-density-wave (CDW) physics among other fundamental properties. Here we report on the existence of a novel structural branch with the general formula $[Ba(PO_4)_2][W_mO_{3m-3}]$ ($m=3$, 4 and 5) denominated *'layered monophosphate tungsten bronzes'* (L-MPTB). It results from thick $[Ba(PO_4)_2]^{4-}$ spacer layers disrupting the cationic metal-oxide 2D units and enforcing an overall trigonal structure. Their symmetries are preserved down to 1.8 K and the compounds show metallic behaviour with no clear anomaly as a function of temperature. However, their electronic structure displays the characteristic Fermi surface of previous bronzes derived from 5*d* W states with hidden nesting properties. By analogy with previous bronzes, such a Fermi surface should result into CDW order. Evidence of CDW order was only indirectly observed in the low-temperature specific heat, giving an exotic context at the crossover between stable 2D metals and CDW order.

[*] H. Nimoh, A. M. Arévalo-López, M. Huvé, O. Mentré
Unité de Catalyse et Chimie du Solide (UCCS), Université de Lille, Centrale Lille/ENSCL
59000 Lille (France)
E-mail: olivier.mentre@univ-lille.fr

H. Nimoh, R. Glaum
Institut für Anorganische Chemie, Rheinische Friedrich-Wilhelms Universität Bonn
Gerhard-Domagk-Str. 1, 53121 Bonn (Germany)
E-mail: rglaum@uni-bonn.de

A. Cano
Institut NEEL CNRS/UGA UPR2940
25 rue des Martyrs, BP 166, 38042 Grenoble (France)

C. Minaud
Institut Michel-Eugène Chevreul, CNRS (FR2638), Université de Lille, Université d'Artois, Centrale Lille, CNRS, l'INRAE
Lille (France)

Introduction

In condensed matter physics and chemistry, the term oxide bronze is used as a generic label to categorize a special class of mixed valent oxides with Na_xWO_3 as original reference materials.[1] Since this early discovery, they have turned into a compulsory family of related mixed valence tungsten and molybdenum oxides, based on the diversity of structural variants and displaying a number of fundamental properties, which most notably include charge-density-wave (CDW) orders assisted by *Peierls* like transitions, as well as superconductivity and some interesting similarities with the high-T_c cuprates. In addition, they also find applications due to their electrochromic[2,3] and catalytic properties after heterovalent mixed-metal (mm) tandem replacing W^V by $(M^{IV}_{1/2}W^{VI}_{1/2})$, $(M^{III}_{1/3}W^{VI}_{2/3})$, or $(M^{II}_{1/4}W^{VI}_{3/4})$.[4,5]

The molybdenum bronzes became very popular in the 80's as they provided the first examples of oxide compounds materializing CDW physics.[6] This was subsequently discovered in the tungsten bronzes, which have become outstanding reference materials ever since.[7] Besides the original A_xWO_3 compounds, only four other major classes of tungsten bronzes have been discovered so far. These are the monophosphate/diphosphate tungsten bronzes with hexagonal (h) tunnels ($MPTB_h$/$DPTB_h$) and the monophosphate/diphosphate tungsten bronzes with pentagonal (p) tunnels ($MPTB_p$/$DPTB_p$), in which hexagonal or pentagonal channel walls are formed from the covalent inclusion of the (di)phosphate groups.[7,8,9] Here, the aforementioned electronic instabilities take place in the WO_3 derivative subunits, with relatively low-symmetry (orthorhombic or monoclinic), which allows for multiple atomic displacive degrees of freedom and symmetry-related electron-phonon couplings.[10] Altogether, these new layered bronzes constitute a versatile material platform of both fundamental and applied interest.

Here we present the structural and electronic properties of an unprecedented series of genuinely layered tungsten monophosphate bronzes with general formula $[Ba(PO_4)_2]W_mO_{3m-3}$ ($m=3$, 4, 5), denominated L-MPTB hereafter. They meet enhanced 2D-criteria due to thick iono-covalent spacers separating the covalent W_mO_{3m-3} blocks, in absence of any h nor p tunnels. As we show below, the $m=4$ member of this series provides the extension of the reference molybdenum bronze $[K(MoO_4)_2]Mo_4O_9$ to the tungsten case.[11,12] Thus, our tungsten prototypes also disclose a more general series with generic formula $[A(XO_4)_2]M_mO_{3m-3}$.

Results and Discussion

The synthesis of the novel L-MPTB materials (single crystals and polycrystalline samples) was performed using a high temperature solid route (see Supplemental Material for further details). Figure 1 illustrates the crystallographic principles and structures across the new L-MPTB series. Hence, they correspond to the scission of $MPTB_h$'s into trigonal tungsten-oxide layers (Figure 1a), where the virtual $m=1$ member corresponds to the β-$[Ba(PO_4)_2][Zr]$[13] structural prototype (Figure 1b). These materials display a ReO_3-type slab of corner sharing WO_3 that is characteristic of previous bronzes, but much more regular along the three pseudo-cubic (perovskite) axis shown in red in Figure 1c. In the title series, the m index corresponds to the number of stacked octahedra along both the trigonal c-axis and the pseudo cubic-axis c_p, which simplifies their structural decoding. The spacer of the new L-MPTB series, however, corresponds to the $Ba(PO_4)_2$ slab and hence is fundamentally different compared to previous tungsten bronzes. This new spacer layer, in particular, tends to enforce a trigonal symmetry to the system as exemplified in the quasi-2D magnets $[Ba(PO_4)_2]M_2$ (M=Co, Ni, Fe).[14–16] The layer thickness $d \approx 5$ Å and ionic character emphasizes a "genuine" 2D-behavior, interrupting electronic interactions between the ReO_3-like layers. This is in fundamental contrast to previous MPTB's built on covalent W–O–P–O–W paths with respect to either orthorhombic or monoclinic structures. However, the total number of d electrons is systematically 2 per m W atoms, which reproduces the same features found in the MPTBp's.[17] We also emphasize that in the $BaO\text{-}P_2O_5\text{-}WO_x$ system, only few $DTPB_h$ $Ba_{\sim 1}P_4O_8(WO_3)_{2m}$ compounds[18] with predominant disordered intergrowths have been reported so far, despite the enormous body of prospective works. It highlights how the initial Ba:P stoichiometric ratio drives the final product and may explain our recent discoveries. The precise structures of the $m=3$, 4 and 5 members of the new L-MPTB series are described in the following. All results are based on single crystal-XRD data. Selected crystallographic information, and extra Rietveld refinement results using polycrystalline samples can be found in Figure S1a–d.

The structure of $[Ba(PO_4)_2]W^{5.33+}{}_3O_6$ ($m=3$) at room temperature crystallizes in the trigonal $R\bar{3}m$ space group ($a=5.2380(2)$ Å, $c=35.464(3)$ Å, $R_F=2.39\,\%$), see Figure 1c. It exhibits a single W–W distance of 3.7073(8) Å with nearly linear W–O–W units (angle = 175.8°). The W atoms, however, are shifted along the crystallographic c-axis towards the center of the ReO_3-like slabs (Figure 1g). This displacement, magnified in Figure 1c, is commonly observed

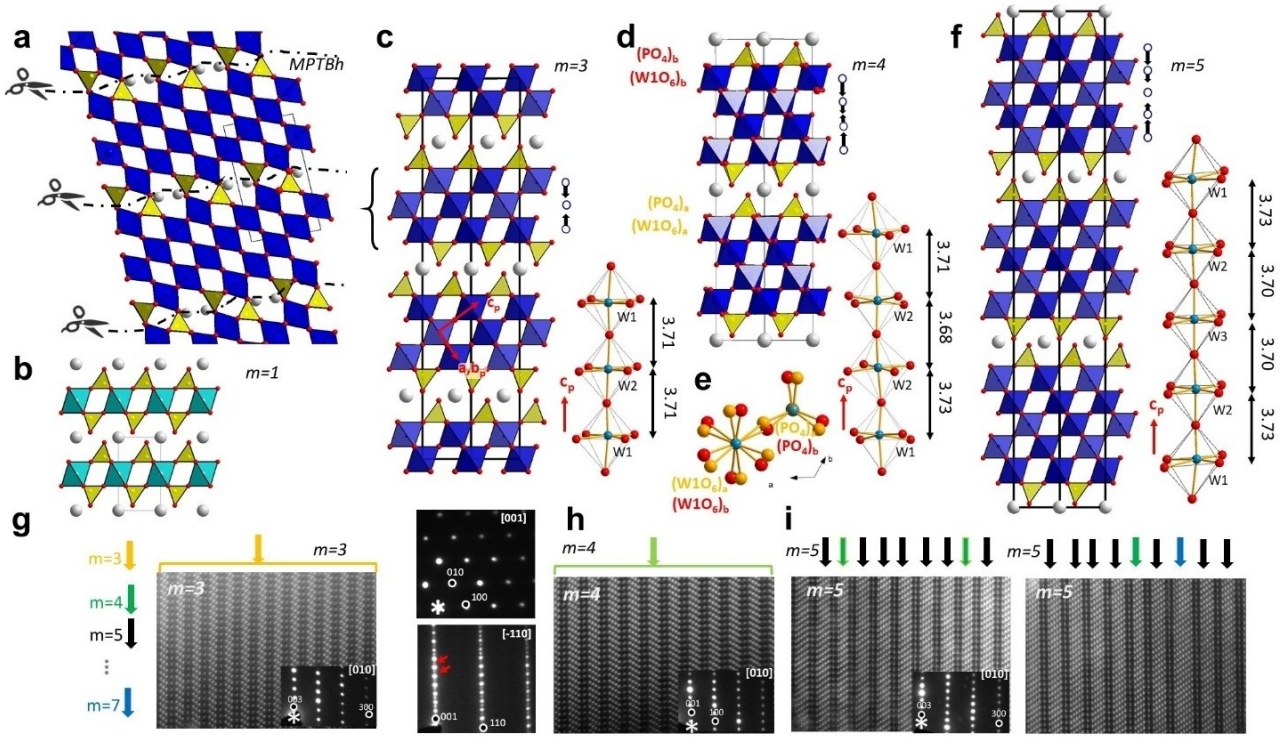

Figure 1. Structural principle of the L-MPTB series. a) Scission of tungsten oxide layers in a parent MPTBh compound. b) $m=1$ β-$[Ba(PO_4)_2][Zr]$ structural analogue. c, e, f) Projection on [110] of the crystal structures for $m=3$, 4, 5 with details of the W shift and m-octahedra long W_mO_{5m+1} row along the perovskite axis. This latter is shown in red for $m=3$. e) $m=4$: eclipsed configurations of the coordination polyhedra between two next 2D-units along c, responsible for the c-axis doubling. g, h, i) HAADF images and [010] ED patterns for $m=3$, 4 and 5. For $m=4$ [001] and [-110] ED patterns are also given, the latter showing the c-doubling. For $m=5$ two HAADF images allow for detection of 2D intergrown structures with $m=4$ and $m=6$ layers.

in previous MPTB's and is related to participation of the external oxide anions in strongly covalent P–O bonds. The WO_6 octahedral tilting reveals an ideal configuration along the perovskites pseudocubic axes (i.e. $a^0b^0c^0$ in the Glazer notation, Figure S3a). Besides, electron diffraction (ED) and high angle annular dark-field scanning transmission electron microscopy (*HAADF*-STEM) reveal the absence of stacking faults in our samples (Figure 1g).

$[Ba(PO_4)_2]W^{5.5+}{}_4O_9$ ($m=4$) displays a more complex structure. At room temperature, its primitive cell is doubled, which corresponds to the $P\bar{3}c1$ space group ($a=5.2092(2)$ Å, $c=2\times14.0812(1)$ Å, $R_F=2.94\,\%$) (Figure 1d). Evidence for the *c*-doubling is provided in the Figure 2a–b. The two-steps structure determination using both 4D (Figure S2) and 3D models is described in detail (See Supplemental Material). It stems from the WO_6 octahedral tilting ($a^-b^-c^-$ Glazer tilt model, Figure S3b) which imperturbably propagates across the $Ba(PO_4)_2$ spacer layer. It results in the alternation along the *c*-axis of two tilted layers, with an eclipsed position of oxygen by ≈20° (Figure 1e). Here again, the W shift in their O_6 octahedra creates a significant dimerization of the central W pair, with $d_{W2\text{-}W2}=3.6826(7)$ Å, against external $d_{W2\text{-}W1}=3.7122(6)$ Å along all intersecting W_4 rows (Figure 1d). HAADF images reveal again neither chemical defects nor stacking faults. However, the [−110] ED pattern allows for a clear observation of the supercell oxygen ordering (Figure 1h). The *c*-doubling is preserved between 110 and 440 K (Figure 2d) while the lattice parameters and W–W distances (refined from both synchrotron powder (SPXRD) and single crystal (SCXRD) X-ray diffraction data between 440 and 120 K) evolve gradually with temperature (Figure 2c–d). Besides the $2\times c$ supercell, the $m=4$ member of the new L–MTPB series represents the tungsten counterpart of the reference molybdenum bronze KMo_6O_{17} ($=[K(MoO_4)_2]Mo_4O_9$) and thus allows to extend the L-MPTB family to $A[XO_4]_2M_mO_{3m-3}$ covering at least A = K, Ba, X = P, Mo, M = Mo, W.

The structure of $[Ba(PO_4)_2]W^{5.6+}{}_5O_{12}$ ($m=5$) crystallizes in the space group $R\bar{3}m$ ($a=5.2292(6)$ Å, $c=48.740(6)$ Å, $R_F=5.29\,\%$), see Figure 1f. As found in the previous case, the W–W distances within the W_5 rows are split, leaving W_3 trimers ($d_{W3\text{-}W2}=3.6949(12)$ Å) and external ($d_{W2\text{-}W1}=3.7298(15)$ Å). In addition, the refined configuration is very close to $a^0b^0c^0$, which preserves a nearly-undistorted metal-oxide block (Figure S3c). We note that single phase polycrystalline $m=5$ material was not prepared, including at best 11.85 % of the $Ba(P_2O_4)_2(WO_3)_{16}$ secondary phase.[19] The ED patterns on selected areas confirmed the existence of large regions with fully ordered $m=5$ L-MPTB. However, we observed the intergrowth of multiple *m* L-MPTBs in the thin part of crystals in the HAADF images (Figure 1i). This suggests a relative chemical instability of this "high" *m* member but also the possibility to extend the series up to $m=7$.

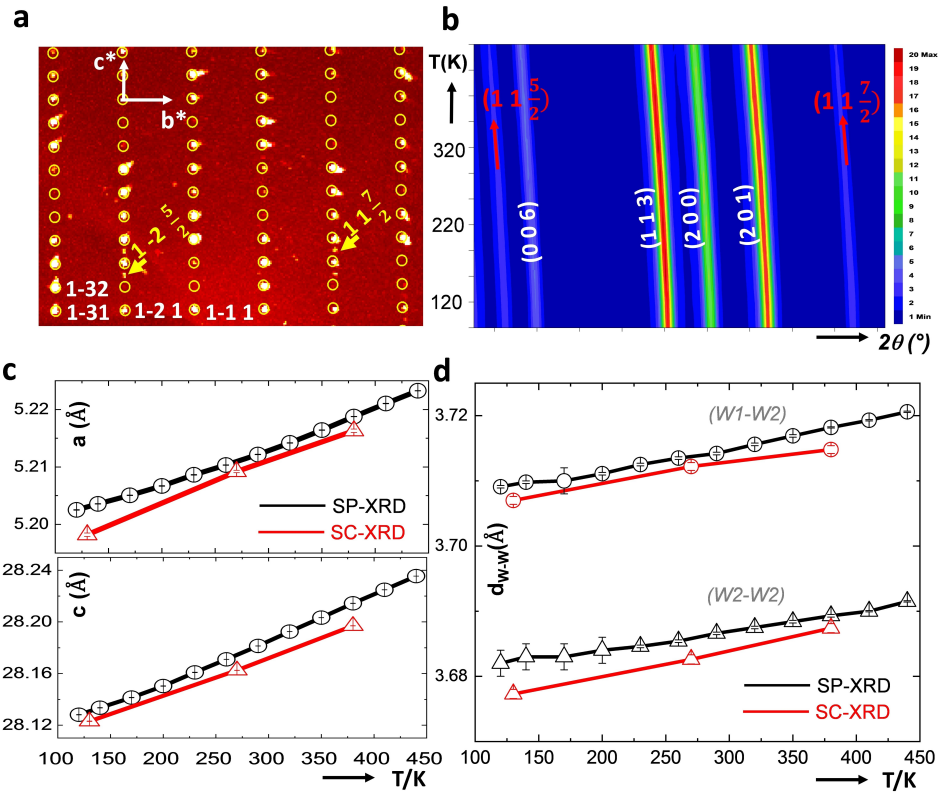

Figure 2. Diffraction and structural features for $m=4$. a) 1kl reconstituted precession frame from SC-XRD data at RT with evidence of 2*c* satellites (yellow). b) Smooth thermal evolution of SPXRD profile with stable 2*c* supercell satellites (red). c–d) Thermal evolution of the lattice parameters and W–W distances for both SP- and SC-XRD experiments.

The structure data are available from CCDC.[20] Generally speaking, independent of the formal metal valences, which are reported in Tables S1b, the bond valence sum (BVS) calculations for the independent W sites of the $m=3$, 4, 5 compounds advocate for increasingly reduced W-ions towards the centre of the metallic slabs, similarly to the findings in previous MPTB's.[9] This BVS gradient is less pronounced as m increases.

Importantly, our structural investigation of the $m=4$ in a broad thermal domain, and on other members of the series at RT, did not give any evidence of CDWs diffraction characteristics such as diffuse-scattering streaks, diffuse background, and/or (in)commensurate modulation satellites, upon the screening of the temperature using electron (77 K-RT), single crystal XRD (130–380 K) and SPXRD (120–440 K). Together with the monotonous contraction of W–W distances on cooling refined for $m=4$, it refutes the occurrence of any sensitive Peierls-like transition in the studied thermal domain. Thus, it differs significantly from previous W bronzes in which W-shift offered by monoclinic and orthorhombic symmetries and modulated features where systematically observed at various temperatures.[9,21,22] Besides the multi-m intergrowth in thin parts mentioned for $m=5$, all compounds show a good crystallinity and the lack of any clues for local disordering.

Similar, in-plane atomic displacements are forbidden by the trigonal symmetry, and may be locked by the rigid $[Ba(PO_4)_2]^{4-}$ interfacial spacers. This argument is corroborated by its relatively large in-plane lattice parameter ($a \approx 5.2$ Å) compared to its reduced value in other inorganic materials, more prone to lattice distortion, e.g. $[Ba(PO_4)_2]Fe_2$ ($a \approx 4.9$ Å) which exhibits a re-entrant trigonal→triclinic Jahn–Teller (JT) distortion around 140 K.[14,23] Beyond W/Mo-bronzes, similar ionic spacers also slice perovskite-blocks, as observed for instance in the hexagonal perovskites 12H-$[Ba(XO_4)_2][Ba_4Na_2M_2O_9]$ (M = Ru, Nb, Ta, Sb; X = V, Cr, Mn, P, As, $P6_3/mmc$ space group) series,[24] or in the 15R-$SrVO_{2.2}N_{0.6}$ (i.e. $[Sr(VO_4)_2]Sr_4V_3O_3N_3]$, $R\bar{3}m$ space group) prepared after nitridation of $SrVO_3$ thin films.[25] In the later metallic phase, an anomaly in the low temperature resistivity was assigned to the possible development of a spin-density-wave instability, which again highlights the specificity of our title series. At least the Ba–O bonds in the interleaves play in favor of enhanced inner ionicity and a more pronounced 2D-nature of the metal oxide blocks than for Sr–O based spacers.[26]

Next, we discuss the transport properties for the L-MPTB series. Figure 3a shows the measured resistivity as a function of the temperature using dense (d > 90 %) as-prepared pellets which consist of agglomerate misoriented crystals. The data reveals a steady metallic behaviour from room temperature down to 1.8 K. For $m=4$ and 5, however, we observe a slight upturn in the very-low temperature regime that we ascribe to sample quality.

Similarly, thermopower measurements reveal a rather conventional behaviour as shown in Figure 3b. In fact, the data can be nicely fitted using a negative-charge carrier thermo-diffusion term (which dominates the high-temperature behaviour) plus a phonon-drag contribution (Supplemental Material and Table S2). In addition, the specific heat as a function of temperature also seems to display a conventional behaviour (Figure 3c). After subtracting the electronic contribution γT ($\gamma = 11.2(9)_{m=3}$, $\gamma = 9.3(3)_{m=4}$, $\gamma = 9.0(2)_{m=5}$ mJ K^{-2} mol^{-1}) see Table S2, the data can be fitted using two Debye scattering contributions (Figure S4). While all data support our structural conclusions, this behaviour of the L-MPTBs is in striking contrast to all the previous MPTB's for which dramatic CDW anomalies are systematically observed about 100 K or above.[9,27] To gain further insight, we performed DFT calculations to determine the electronic structure of the new L-MPTBs (see Supplemental Material for details). Figure 4a and b shows the computed Fermi surface (FS) and band structure for the $m=3$, 4 and 5 members of the L-MPTB series. These FSs have a remarkable 2D character and display the characteristic topology found in previous bronzes.[10,12] Specifically, the three different FS sheets can be associated with one of the three bands at the bottom of the 5*d*-W manifold that crosses the Fermi level (Figure 4b).

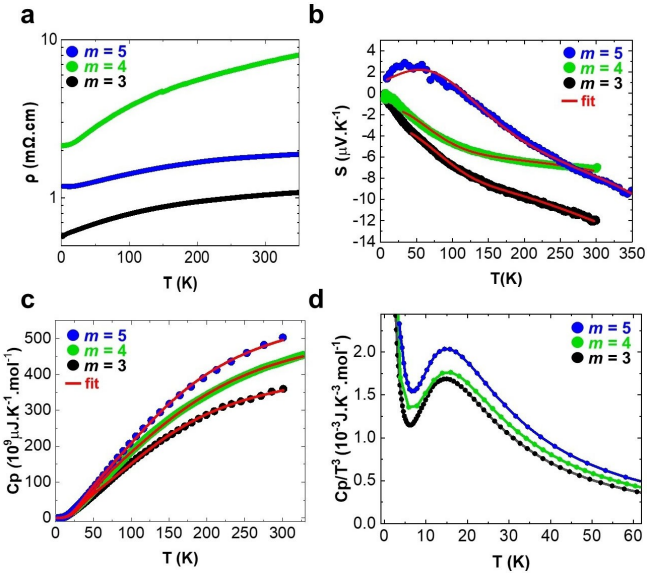

Figure 3. Physical properties of the L-MPTB series ($m=3$, 4, 5) versus temperature and fit following the main text. a) resistivity b) thermopower c) lattice contribution of the heat capacity. d) Cp/T^3. The $m=5$ sample contains 10 wt% of an impurity.

These partially filled bands relate to the t_{2g} states of the WO_6 octahedra and contain sizeable contributions of the independent W atoms in the ReO_3-like slab as shown in their density of states (DOS), after normalization by the site multiplicity (Figure 4c). The strongest electronic participation of the central W atoms is reminiscent of the BVS partition discussed above. At the same time, the FSs shown in Figure 4a may appear from hidden 1D FS with nesting properties This concept was introduced by Canadell and Whangbo,[10,12] where the 2D-FS cannot explain the experimental CDW nesting vectors. Instead, they can be understood as a superposition of 3 sets of nested quasi-1D surfaces which form parallel lines. In real space they correspond to three sets of weakly coupled conductive zigzag chains of

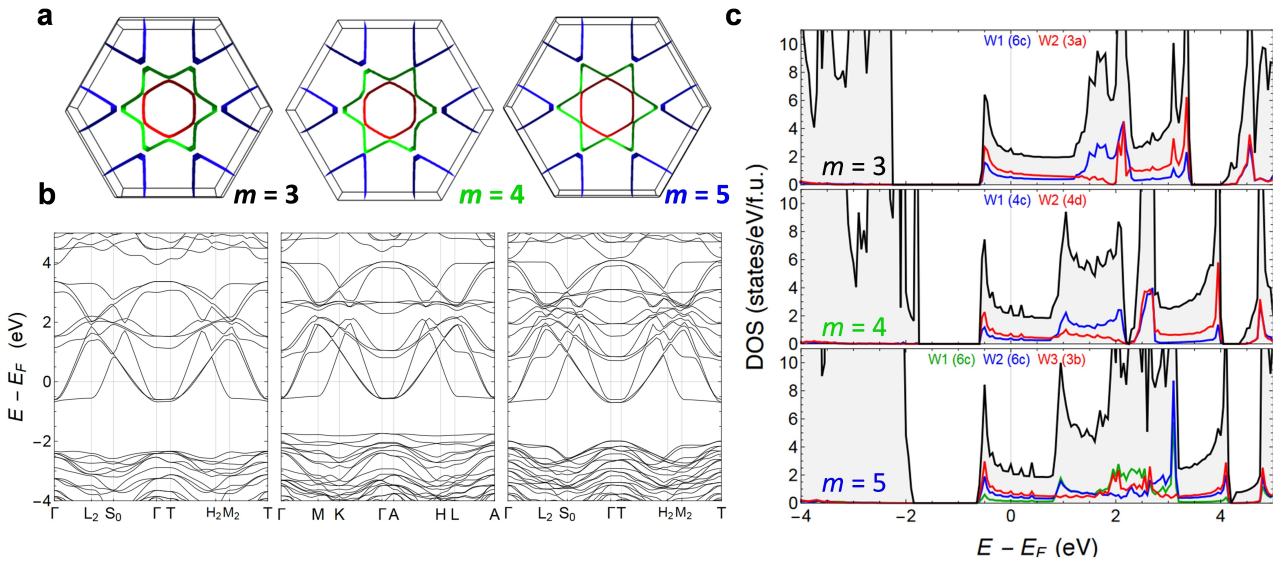

Figure 4. DFT calculation. a) Fermi surfaces and b) electronic band structure calculated for the $m = 3$, 4, and 5 members of the MTPB series $[Ba(PO_4)_2]W_mO_{3m-3}$ (see Supplemental Material for details). The Fermi surface of these systems has a remarkable 2D character. The three different sheets of these Fermi surfaces are associated with the three different bands that cross the Fermi level in the corresponding band plots. These half-filled bands belong to the 5*d*-W manifold that extend from ≈ -0.5 eV to $\approx +4$ eV. c) Corresponding Density-of-states (DOS) (black curves) and projected 5*d*-W DOS (the different Ws are labelled according to their Wyckoff positions, see Table S1c). The DOS at the Fermi level is essentially due to the 5*d* contributions of the W atoms, with sizeable contributions from all of them.

corner-sharing WO_6 octahedra running parallel to the 2D-plane, with t_{2g} orbital characters. Therefore, the electronic structure of the new L-MPTB series should, by analogy, be prone to the same type of CDW instabilities. This expectation, however, is at odds with the experimental data discussed above, which shows no sign of CDW distortion neither in the structure nor in transport, thermopower, and specific heat measurements.

To further test the possibility of CDW order we take a closer look at the specific heat data at low temperatures since this may provide some evidence like in the potassium-molybdenum counterpart of our $m = 4$ system KMo_6O_{17}.[28] Figure 3d shows $C_P/T^3(T)$ plots which reveal a hump at ≈ 15 K followed by an upturn on cooling that roughly scales as T^{-2}. These features are systematically observed in CDW systems and are characteristic of phason- excitations.[29,30] Specifically, the hump is associated to the amplitude mode of the CDW—with an extra contribution from the phason mode if this latter one is also gapped—while the upturn derives from the finite lifetime of the phase mode. Thus, the antagonist situation deduced from our structural and physical measurements—where we find no evidence of CDW—and the specific-heat data—where CDW features are visible—suggests the possibility of a different, novel electronic state related to the enhanced two-dimensionality of our systems.

Conclusion

In summary, we have synthesized a whole new series of monophosphate tugnsten bronzes that display some analogies but also major differences compared to previous bronzes. The main novelty of this series emerges from the thick $Ba(PO_4)_2$ spacer with ionic Ba–O bonds, slicing regular WO_3-like layers with enhanced 2D character which seems to lock an overall trigonal symmetry. Interestingly, the structure of the reference molybdenum bronze KMo_6O_{17} is extended within the new series to the tungsten case, thereby disclosing a broader family of materials with generic formula $[A(XO_4)_2]M_mO_{3m-3}$. The electronic structures of the new bronzes have a pronounced 2D character with hidden Fermi surface nesting. However, the crystal structures of these systems remain unchanged as a function of temperature and they remain metallic with no CDW signatures in the structure, resistivity or thermopower. In contrast, the structural origin of the systematic CDWs reported in former bronzes fingerprint electronic localizations along specific nesting vectors. They are often interpreted as Peierls-like transitions with significant basal W shifts allowed in the orthorhombic/monoclinic symmetries[9,21] but forbidden in the trigonal symmetry. Again, the influence of the rigid $Ba(PO_4)_2$ spacer layer may be involved in the temperature preserved crystal system. Strikingly, evidence of locked/hidden low-temperature CDW excitations is observed in the specific heat of these new compounds. This puzzling situation is expected to motivate further investigations of this type of oxide bronzes in relation to their electronic instabilities and emergent orders.

Acknowledgements

We thank support from ANR AMANTS project (19-CE08-0002-01) and the ILL (C. Ritter) and ALBA (F. Fauth) for beamtime at D20 and MSPD respectively. The Chevreul Institute (FR 2638), Region Hauts-de-France, and FEDER are acknowledged for funding the X-ray diffractometers and the PPMS magnetometer. Laurence Burylo and Nora Djellal at the UCCS are also acknowledged for for their experimental contribution. Open Access funding enabled and organized by Projekt DEAL.

Conflict of Interest

The authors declare no competing interests.

Data Availability Statement

The data that support the findings of this study are available from the corresponding author upon reasonable request.

Keywords: 2D Metals · Charge-Density Waves · Fermi Surfaces · Mixed-Valence Oxides · Transition-Metal Oxides

[1] F. Wöhler, *Philos. Mag.* **1825**, *66*, 263–269.
[2] E. Masetti, D. Dini, F. Decker, *Sol. Energy Mater. Sol. Cells* **1995**, *39*, 301–307.
[3] A. Zimmer, M. Gilliot, M. Tresse, L. Broch, K. E. Tillous, C. Boulanger, N. Stein, D. Horwat, *Opt. Lett.* **2019**, *44*, 1104–1107.
[4] S. C. Roy, W. Assenmacher, T. Linden, L. Esser, W. Mader, R. Glaum, *Z. Naturforsch. B* **2016**, *71*, 543–552.
[5] A. Karbstein, M. Weber, D. Lahr, J. Daniels, W. Assenmacher, W. Mader, F. Rosowski, S. A. Schunk, R. Glaum, *Eur. J. Inorg. Chem.* **2021**, 1459–1469.
[6] J. Dumas, C. Schlenker, *Int. J. Mod. Phys. B* **1993**, *7*, 4045–4108.
[7] M. Greenblatt, *Acc. Chem. Res.* **1996**, *29*, 219–228.
[8] M. Greenblatt, *Molybdenum and Tungsten Bronzes, in Physics and Chemistry of Low-Dimensional Inorganic Conductors* (Eds.: C. Schlenker, J. Dumas, S. van Smaalen), NATO ASI Series, *Vol. 354*, Springer, Boston, **1996**, pp. 15–43.
[9] P. Roussel, O. Pérez, P. Labbe, *Acta Crystallogr. Sect. B* **2001**, *57*, 603–632.
[10] E. Sandre, P. Foury-Leylekian, S. Ravy, J. P. Pouget, *Phys. Rev. Lett.* **2001**, *86*, 5100–5103.
[11] H. Vincent, M. Ghedira, J. Marcus, J. Mercier, C. Schlenker, *J. Solid State Chem.* **1983**, *47*, 113–121.
[12] M. H. Whangbo, E. Canadell, P. Foury, J. P. Pouget, *Science* **1991**, *252*, 96–98.
[13] D. Bregiroux, R. Jardin, K. Popa, P. E. Raison, G. Wallez, M. Quarton, M. Brunelli, C. Ferrero, R. Caciuffo, *J. Solid State Chem.* **2009**, *182*, 1115–1120.
[14] H. Kabbour, R. David, A. Pautrat, H. J. Koo, M. H. Whangbo, G. André, O. Mentré, *Angew. Chem. Int. Ed.* **2012**, *51*, 11745–11749; *Angew. Chem.* **2012**, *124*, 11915–11919.
[15] N. Faza, W. Treutmann, D. Babel, *Z. Anorg. Allg. Chem.* **2001**, *627*, 687–692.
[16] P. Regnault, J. Rossat-Mignod, L. J. de Jongh, *Magnetic Properties of Layered Transition Metal Compounds, Vol. 9*, Kluwer Academic Publishers, Amsterdam, **1990**, pp. 271–318.
[17] M. Greenblatt, in *Crystal Chemistry and Properties of Materials with Quasi-One-Dimensional Structures*, pp 15-45 NATO ASI series B: physics Vol. 354, **1996**, Plenum Press, New York.
[18] B. Domengès, M. Hervieu, B. Raveau, *Acta Crystallogr. Sect. B* **1984**, *40*, 249–256.
[19] M. Lamire, P. Labbé, M. Goreaud, B. Raveau, *J. Solid State Chem.* **1987**, *71*, 342–348.
[20] Deposition numbers 2227054, 2227055 and 2227056 contain the supplementary crystallographic data for this paper. These data are provided free of charge by the joint Cambridge Crystallographic Data Centre and Fachinformationszentrum Karlsruhe Access Structures service.
[21] A. Ottolenghi, J. P. Pouget, *J. Phys. I* **1996**, *6*, 1059–1083.
[22] P. Roussel, P. Labbé, H. Leligny, D. Groult, P. Foury-Leylekian, J. P. Pouget, *Phys. Rev. B* **2000**, *62*, 176.
[23] R. David, A. Pautrat, D. Filimonov, H. Kabbour, H. Vezin, M. H. Whangbo, O. Mentré, *J. Am. Chem. Soc.* **2013**, *135*, 13023–13029.
[24] E. Quarez, F. Abraham, O. Mentré, *J. Solid State Chem.* **2003**, *176*, 137–150.
[25] T. Yamamoto, A. Chikamatsu, S. Kitagawa, N. Izumo, S. Yamashita, H. Takatsu, M. Ochi, T. Maruyama, M. Namba, W. Sun, T. Nakashima, F. Takeiri, K. Fujii, M. Yashima, Y. Sugisawa, M. Sano, Y. Hirose, D. Sekiba, C. M. Brown, T. Honda, K. Ikeda, T. Otomo, K. Kuroki, K. Ishida, T. Mori, K. Kimoto, T. Hasegawa, H. Kageyama, *Nat. Commun.* **2020**, *11*, 5923.
[26] R. Souda, K. Yamamoto, W. Hayami, T. Aizawa, Y. Ishizawa, *Phys. Rev. B.* **1994**, *50*, 4733–4738.
[27] C. Schlenker, C. Hess, C. le Touze, J. Dumas, *J. Phys. I* **1996**, *6*, 2061–2078.
[28] J. Wang, R. Xiong, D. Yin, C. Li, Z. Tang, Q. Wang, J. Shi, Y. Wang, H. Wen, *Phys. Rev. B* **2006**, *73*, 235409.
[29] G. Reményi, S. Sahling, K. Biljaković, D. Starešinić, J. C. Lasjaunias, J. E. Lorenzo, P. Monceau, A. Cano, *Phys. Rev. Lett.* **2015**, *114*, 195502.
[30] A. Cano, A. P. Levanyuk, *Phys. Rev. Lett.* **2004**, *93*, 245902.

Manuscript received: February 13, 2023
Accepted manuscript online: April 6, 2023
Version of record online: May 9, 2023